Ramsey-fringe shape in an alkali-metal vapor cell with buffer gas

Salvatore Micalizio, Claudio E. Calosso, Filippo Levi, and Aldo Godone
Istituto Nazionale di Ricerca Metrologica, INRIM, Strada delle Cacce 91, 10135 Torino, Italy
(Received 30 May 2013; published 3 September 2013)

In this paper we describe a few phenomena that may affect the linewidth and/or the line shape of Ramsey fringes observed in an alkali-metal vapor cell with buffer gas. Experiments are performed on a vapor-cell–microwave-cavity arrangement in which ^{87}Rb atoms successively experience laser pumping preparation (through a D_2 line), microwave interrogation with a couple of coherent pulses, and clock signal detection by means of laser absorption. We show that the linewidth of the Ramsey central fringe is influenced by the Rabi pattern produced by a single microwave pulse. Moreover, cycle memory and atomic density effects can modify the shape of the Ramsey central fringe from the common sinusoidal behavior. A simple three-level model well reproduces the experimental observations.

DOI: 10.1103/PhysRevA.88.033401 PACS number(s): 32.80.Xx, 06.30.Ft, 32.30.Bv

I. INTRODUCTION

Since its introduction in the 1950s, the Ramsey method of separated oscillatory fields [1] proved to be an invaluable tool in high-resolution atomic and molecular spectroscopy. Originally conceived for molecular and atomic beams [2], over the years, Ramsey fringes have been observed in several atomic systems, such as cold atoms [3] and single trapped ions [4], and adopting different excitation schemes, including Doppler-free two-photon resonance [5], polarization rotation [6], and ground-state Zeeman coherence [7].

Basically, in any Ramsey-like experiment, a first electromagnetic pulse of duration t_1 excites a coherence oscillating at the transition frequency ν_0 (atomic Bohr's frequency). A second pulse, delayed by T and with a precise phase relation to the first pulse, probes the atomic coherence. Accordingly, any physical observable related to the excitation will exhibit a typical interference pattern (Ramsey fringes) with an amplitude dependent on the phase difference between the atomic coherence and the probe field.

It is well known that the Ramsey interaction exhibits several features particularly interesting for high-resolution spectroscopy applications. Provided $t_1 \ll T$, the shape of the central fringe is proportional to $\cos(\Omega_\mu T)$, where $\Omega_\mu \equiv 2\pi(\nu - \nu_0)$ is the (angular) microwave detuning, ν being the frequency of the interrogating microwave signal. Moreover, the linewidth $\Delta\nu_{1/2}$ of the central fringe depends on T through the relation,

$$\Delta\nu_{1/2} = 1/2T, \tag{1}$$

and is, in principle, immune to any microwave and/or laser power broadening. These properties are fully exploited in current primary frequency standards, such as cesium-beam clocks and cesium atomic fountains.

The possibility to implement a compact and high-performing clock also suggested the application of the Ramsey technique to vapor-cell devices.

To our knowledge, the first work in this regard dates back to the 1960s [8] where two time-separated phase-coherent microwave pulses were used to observe the 0-0 hyperfine transition of a Rb gas cell clock, reducing, at the same time, the frequency shift caused by the pumping light. Recently, also thanks to the development of laser diodes as optical pumping sources, Ramsey fringes in a hot atomic vapor have been studied for clock applications using an all-optical interaction (see, for example, Ref. [9]) or a more traditional double-pulse (microwave plus laser) approach [10–13]. In particular, ultrahigh contrast resonances leading to remarkable improvement in the signal-to-noise ratio have been detected in Ref. [12], whereas, record results in terms of frequency stability have been reported in Ref. [13].

The purpose of this paper is to describe a few phenomena that may affect the Ramsey central fringe (RCF) observed in an alkali-metal vapor cell with buffer gas. Specifically, we show that, in ordinary laboratory conditions, $\Delta\nu_{1/2}$ may also deviate significantly from Eq. (1) and the RCF shape may diverge from the pure sinusoidal behavior.

The first point we discuss in the paper is the residual effect of the Rabi interaction on the RCF. Although this is a well-known phenomenon [14], we will make clear that, because of relaxation, the condition $t_1 \ll T$ is not always well satisfied in a buffered cell and the RCF turns out better approximated including a contribution depending on the microwave amplitude.

Moreover, we report on the study of nonlinear effects that contribute to the shape of the RCF. Specifically, high-order harmonics appear in the Ramsey pattern, and the RCF is no more a pure cosine function of Ω_μ. This nonlinear behavior may be due to two different physical causes. The first one is related to the incomplete extinction of the atomic coherence in the ground state between one operation cycle and the following one. This "phase memory" is responsible for the residual light shift in a pulsed optically pumped (POP) clock and has extensively been discussed elsewhere [15,16]. Here we show that the atomic population may also suffer for a not complete separation among the different operation phases of the POP clock, leading to a not so elementary shape of the RCF.

The second effect is related to the optical thickness of the atomic sample. We observed, in fact, that the amplitude of high-order harmonics depends on the temperature (and then on the atomic density).

The paper is organized as follows. In Sec. II, we will introduce the theoretical model we adopted to reproduce the observed phenomenology; this analysis is based on a simple three-level system. In Sec. III, we will describe the experimental setup, whereas, in Sec. IV, we will describe the

experimental results and their interpretation in terms of the model developed in Sec. II. Discussion and conclusions will be reported in Sec. V.

II. THEORETICAL MODEL

The atomic system we consider is a vapor of ^{87}Rb atoms in a cell with buffer gas.

We suppose observing Ramsey fringes through the sequence of the three phases (optical pumping, microwave interrogation, and laser absorption detection) that commonly rule the operation of the POP clock, even though the effects we will describe can easily be extended to other techniques used to excite Ramsey fringes in a buffered cell, such as pulsed-coherent population trapping or push-pull-Ramsey interactions [17].

The first phase is the optical pumping that we suppose performed by an intense laser pulse that prepares the atoms, producing a large population imbalance in the two ground-state hyperfine levels of ^{87}Rb. The laser is tuned to a D_1 or D_2 optical line, and its wave vector is parallel to the quantization axis defined by a static magnetic field $\mathbf{B}_0 = B_0\hat{\mathbf{z}}$. The two circular polarization components σ^+ and σ^- of the linearly polarized laser couple the $\Delta m_F = 1$ and $\Delta m_F = -1$ sublevel transitions, respectively, according to the scheme of Fig. 1(a) (which shows the complete Zeeman-level structure in the case of D_2).

It is well established that relaxation processes (such as buffer gas collisions, spin exchange, and cell-wall collisions) induce a well-precise dynamics among Zeeman sublevels of the Rb ground state. The quantities we are interested in, the population inversion among the two clock levels ($|2\rangle = |F{=}1, m_F = 0\rangle$ and $|6\rangle = |F = 2, m_F = 0\rangle$) and the coherence between them, are, in principle, coupled to other ground-state sublevels as it turns out from Liouville's equation [11].

However, to gain more physical insight without recurring to numerical simulations, we consider an equivalent three-level system composed of the two clock levels and an excited state.

Besides simplifying the equations, this approach is motivated by the fact that the atom-microwave interaction, mainly responsible for the Ramsey shape, reduces to a two-level system (levels $|2\rangle$ and $|6\rangle$) also in the presence of a ground-state Zeeman structure [11]. The other levels, in fact, play a role during the optical pumping and the detection times only.

Reducing the multilevel scheme of Fig. 1(a) to the simpler one of Fig. 1(b) requires, nevertheless, a phenomenological rescaling of the values of the main parameters, especially if we intend to compare theoretical predictions with experimental results.

As already performed in Ref. [18], we introduce an effective atomic density n_{eff} so that $n_{\text{eff}} = kn$, where n is the actual atomic density and k is a phenomenological coefficient taking into account that not all the atoms in the ground state are involved in the interaction process. Basically, k is related to the maximum steady-state value (averaged all over the entire cell) that the population inversion may achieve at the end of the pumping phase. According to the scheme of Fig. 1, k can be, at most 1/3, but its value in a specific situation actually depends on many physical parameters, such as laser power and absorption, and on the technique adopted to perform optical

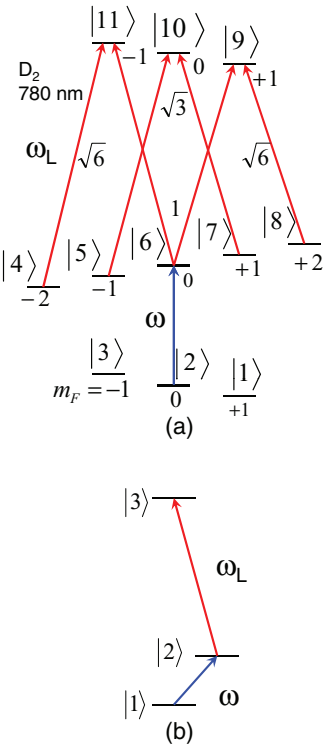

FIG. 1. (Color online) (a) Atomic levels of ^{87}Rb involved in the POP clock operation; (b) reduced three-level system. ω_L and ω are the laser and microwave angular frequencies; the relative strengths of the different components of the D_2 line are also shown.

pumping (see, for example, the end of Sec. IV C). In our case, the experimental results are well reproduced for $k = 0.2$. All the other quantities related to n, such as the linear absorption coefficient α or the optical thickness of the medium ζ, are rescaled accordingly.

Moreover, the pumping rate Γ_p should also be rescaled; it is related to the laser intensity I_L through the relation,

$$\Gamma_p = \frac{Z_0}{\Gamma^*}\left(\frac{d_e}{\hbar}\right)^2 I_L, \tag{2}$$

where d_e is the electric dipole moment of the optical transition, Z_0 is the impedance of free space, Γ^* is the relaxation rate of the excited state, and $\hbar$ is the reduced Planck constant. From the optical relative transition strengths reported in Fig. 1(a) for D_2, the portion of laser intensity involving the clock level is 1/10 of the total so that the effective pumping rate is as follows:

$$\Gamma_p^{\text{eff}} = \frac{\Gamma_p}{10}, \tag{3}$$

Γ_p being the actual pumping rate evaluated according to Eq. (2).

In the following, unless otherwise specified, we will always refer to an effective pumping rate, and for convenience, we drop the superscript.

In the formalism of the ensemble-averaged density matrix $\hat{\rho}$ [ρ_{ii} atomic populations, ρ_{ij} atomic coherences for $i \neq j$, $i, j = 1$–3 where the atomic levels have been labeled according to Fig. 1(b)] and in the rotating-wave approximation, the optical pumping phase is described by the following set of

Maxwell-Bloch equations:

$$\dot{\Delta}_{\rm pump} + (\gamma_1 + \Gamma_p)\Delta_{\rm pump} = -\left(\frac{n_{\rm eff}}{n}\right)_p \Gamma_p,$$
$$\frac{\partial \Gamma_p}{\partial z} = -\frac{\alpha}{\Gamma^*}\Gamma_p(1 + \Delta_{\rm pump}), \tag{4}$$

where $\Delta = \rho_{22} - \rho_{11}$ is the population inversion among the two clock levels and γ_1 is the longitudinal relaxation rate. The subscript pump is added to distinguish the pumping phase from the successive ones. At the beginning, the atoms are equally distributed among the sublevels; the initial condition for the population inversion is then $\Delta_{\rm pump}(t = 0) = 0$.

The factor $(\frac{n_{\rm eff}}{n})_p$ on the right-hand side of Eq. (4) has been introduced to phenomenologically limit the value of the population inversion at the end of the pumping phase ($|\Delta| \leqslant \frac{1}{3}$).

After the pumping phase, the atoms are interrogated by means of a couple of microwave pulses of duration t_1 separated by a time T. The cell is then supposed to be placed in a microwave cavity where a standing-wave field is applied to the atoms at a frequency corresponding to the hyperfine transition (6.834 GHz). Since we are interested in observing the Ramsey fringes in the frequency domain, the population inversion at the end of the second pulse can conveniently be written as a function of the microwave detuning Ω_μ [14,15],

$$\Delta_{\rm Ramsey}(\Omega_\mu) = \Delta_{\rm pump}(t_p)\left[\frac{e^{-\gamma_1 T}\left(\Omega_\mu^2 + b^2\cos\theta\right)^2}{\xi^4} + \frac{b^2 e^{-\gamma_2 T}\Omega_\mu^2\cos(\Omega_\mu T)(1-\cos\theta)^2}{\xi^4}\right.$$
$$\left. + \frac{2b^2 e^{-\gamma_2 T}\Omega_\mu \sin(\Omega_\mu T)(1-\cos\theta)\sin\theta}{\xi^3} - \frac{b^2 e^{-\gamma_2 T}\cos(\Omega_\mu T)\sin^2\theta}{\xi^2}\right], \tag{5}$$

where $\Delta_{\rm pump}(t_p)$ is the population inversion at the end of the pumping phase, γ_2 is the relaxation rate of the ground-state coherence, b is the microwave Rabi frequency, $\xi = \sqrt{b^2 + \Omega_\mu^2}$, and $\theta = \xi t_1$.

Finally, the atoms that have made the clock transition are detected (subscript det) with a laser probe pulse of duration t_d. This phase is then described by the equations,

$$\dot{\Delta}_{\rm det} + (\gamma_1 + \Gamma'_p)\Delta_{\rm det} = -\left(\frac{n_{\rm eff}}{n}\right)_p \Gamma'_p,$$
$$\frac{\partial \Gamma'_p}{\partial z} = -\frac{\alpha}{\Gamma^*}\Gamma'_p(1 + \Delta_{\rm det}), \tag{6}$$

where Γ'_p is the optical pumping rate during the detection.

We notice that, of course, equations for pumping and detection are formally identical, but in the first case, an intense laser pulse is required to create a large population unbalance between the two clock levels, whereas, in the second case, the laser pulse is used as a probe, and it is expected not to change the population inversion; this is expressed mathematically by the condition,

$$\left(\gamma_1 + \Gamma_p^{\rm det}\right)t_d \ll 1. \tag{7}$$

Under this hypothesis and for a thin atomic medium, Eqs. (6) can be integrated easily, taking the expression given by Eq. (5) as the initial condition for $\Delta_{\rm det}$,

$$\Gamma'_p(z = L) = \Gamma'_p(z = 0)\{1 - \zeta[1 + \Delta_{\rm Ramsey}(\Omega_\mu)]\}, \tag{8}$$

where $\zeta = \alpha L/\Gamma^*$ is the optical length of the cell ($\zeta \ll 1$ for a thin medium) and $\Gamma'_p(z = 0)$ is the detection pumping rate at the entrance of the cell.

It is then supposed that these phases repeat cyclically; in the ideal case, no memory is kept between one cycle and the successive one.

In Sec. IV B, we will remove this hypothesis, whereas, in Sec. IV C, we will analyze the case of a thick atomic medium.

III. EXPERIMENTAL SETUP

In this section, we describe the main elements that compose our experimental setup (Fig. 2); more details can be found in Ref. [13].

The experiments have been performed using a quartz cell of length $L = 20$ mm containing a vapor of isotopically enriched ^{87}Rb and a mixture of buffer gases Ar and N_2 in the pressure ratio 1.6 and with a total pressure of 3333 Pa (25 Torr). The relaxation rates are, of course, affected by the interaction with the buffer gas. In particular, the excited state is homogeneously broadened, and the associated relaxation rate Γ^* is on the order of 3×10^9 s^{-1}. At the temperature of 338 K, for the ground-state relaxation rates, we have $\gamma_1 \approx 360$ and $\gamma_2 \approx 340$ s^{-1}.

The cell is placed in a TE_{011}-mode microwave cavity, which is surrounded by a solenoid producing a constant longitudinal magnetic field of 2 μT. This field provides a quantization axis and removes the Zeeman degeneracy. The cell and the cavity are placed inside three cylindrical μ-metal shields to isolate the cell-cavity arrangement from external magnetic fields. The cell temperature is varied from 318 to 348 K; the atomic density of ^{87}Rb is controlled by the temperature of the cell's stem that

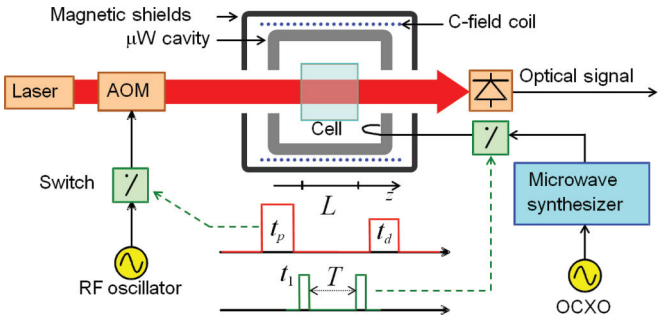

FIG. 2. (Color online) Schematic of the setup used in the experiments; the figure also shows a cycle timing sequence.

is kept at a temperature lower than that of the cell's body as described in Ref. [13].

The laser light is frequency locked to the saturated absorption signal of the $|F = 2\rangle \rightarrow |F' = 1\rangle$ transition of the D_2 line observed in a cell containing only Rb (not shown in the figure). The light is sent to the clock cell through an acoustic-optic modulator (AOM), which acts as an optical power control and switch. The laser power during pumping and detection is changed through the rf signal intensity driving the AOM. In particular, during the pumping phase, the laser intensity I_L is adjusted around 2 mW/cm^2, corresponding to $\Gamma_p \approx 200\,000\ \mathrm{s}^{-1}$, whereas, during detection, the laser intensity is about 0.2 mW/cm^2 ($\Gamma'_p \approx 20\,000\ \mathrm{s}^{-1}$). We adopted these values for the pumping rates in all our experiments and the corresponding effective values in the calculations.

The light transmitted through the cell is detected with a photodiode placed outside the cavity.

The two phase-coherent microwave pulses at 6.834 GHz, required by the Ramsey interrogation scheme, are provided by a low phase-noise synthesis chain (see Ref. [19]).

IV. RESULTS AND INTERPRETATION

In this section, we report the experimental results related to the observation of three phenomena that affect the RCF observed on the laser absorption signal. Their interpretation on the basis of the theoretical model developed in Sec. II is also given.

A. Residual Rabi interaction effect

We consider Eqs. (8) and (5) that describe the Ramsey fringes superimposed on the Rabi pedestal in a thin atomic medium.

A simplified expression for the RCF can be found provided the condition $|\Omega_\mu| \ll b$ is satisfied [14], that is, when $t_1 \ll T$; it is sufficient, in this case, to develop Eq. (5) around $\Omega_\mu = 0$, only keeping the zero-order term in Ω_μ/b. For $\theta = \pi/2$ pulses, we find the expression for the RCF in a cell with buffer gas [15],

$$\Delta_{\mathrm{Ramsey}}(\Omega_\mu) \approx -\Delta_{\mathrm{pump}}(t_p) e^{-\gamma_2 T} \cos(\Omega_\mu T). \tag{9}$$

If, instead, we keep the first term in Ω_μ/b, for $\pi/2$ pulses, we obtain

$$\Delta_{\mathrm{Ramsey}}(\Omega_\mu) \approx -\Delta_{\mathrm{pump}}(t_p)\, e^{-\gamma_2 T} \cos[\Omega_\mu(T + 4t_1/\pi)]. \tag{10}$$

In Fig. 3, we report the RCF (black dots) as observed at the low-temperature regime ($T_K = 318$ K, $\zeta \simeq 0.8$). In order to reduce the noise affecting the signal, each point is the average of 30 values. In the same figure, we report the fitting of the experimental values with Eq. (9) (continuous line) and with Eq. (10) (dashed line) as well.

Besides fitting the experimental behavior better, Eq. (10) also predicts the correct value (147 Hz in our case) for the linewidth of the RCF, which results more properly expressed by the relation,

$$\Delta\nu_{1/2} = \frac{1}{2(T + 4t_1/\pi)}, \tag{11}$$

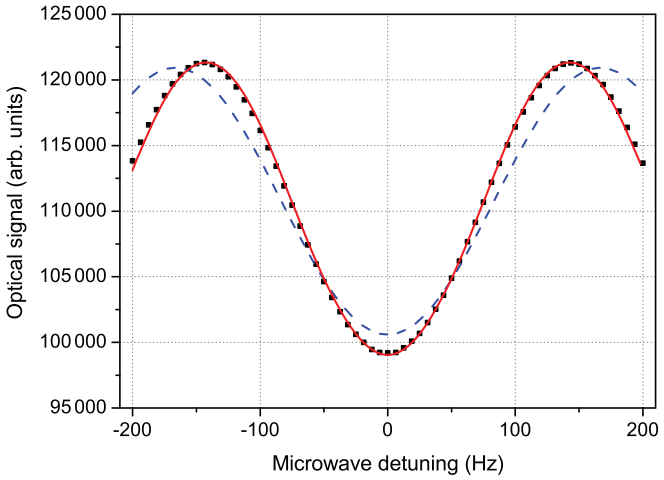

FIG. 3. (Color online) Black dots: experimental data at 318 K (low-temperature regime); continuous line: fit with $\cos[\Omega_\mu(T + 4t_1/\pi)]$; dashed line: fit with $\cos(\Omega_\mu T)$; $t_p = 4$ ms, $t_d = 150\ \mu$s, $T = 3$, $t_1 = 0.4$ ms.

whereas, according to Eq. (1), we would expect a linewidth of about 20 Hz larger.

B. Cycle memory effect

Figure 4 shows the RCF in the same conditions as Fig. 3, except for the pumping time that is now $t_p = 400\ \mu$s.

Compared to Fig. 3, it is evident that the contrast of the fringe is slightly lower, and the minimum appears flattened. Although it is reasonable to attribute the contrast reduction to a smaller value of population inversion generated during the pumping phase, the emergence of a flattened minimum is not immediately clear. The fit of the experimental data with a simple cosine curve (gray line in Fig. 4) results inadequately to correctly describe the observed behavior.

To understand the physics involved in this effect, we start to analyze the case of pumping and detection times much

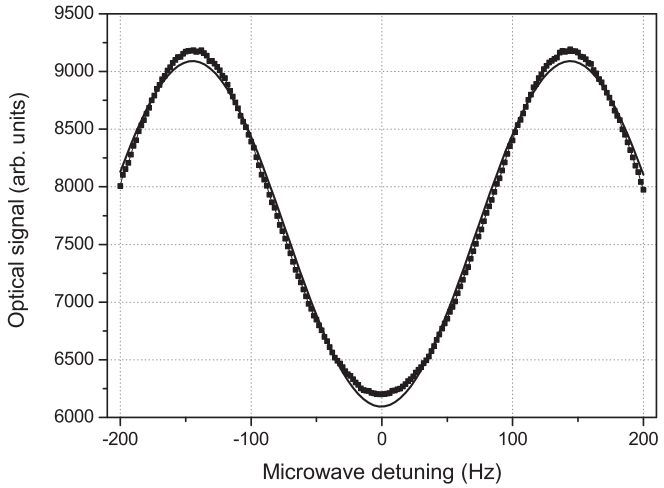

FIG. 4. RCF detected for the following values of the timing parameters: $t_p = 0.4$ ms, $t_d = 150\ \mu$s, $T = 3$, and $t_1 = 0.4$ ms. Gray line: fit of the experimental data with a cosine function of $\Omega_\mu(T + 4t_1/\pi)$.

shorter than γ_1^{-1} so that we can neglect the buffer gas role with a significant simplification of the equations. Moreover, we remind that the signal is an average of contributions coming from a certain number of consecutive operation cycles. For simplicity, we initially only consider two cycles. For the first cycle, labeled with the superscript $^{(1)}$, Eq. (4) becomes

$$\dot{\Delta}^{(1)}_{\rm pump} + \Gamma_p \Delta^{(1)}_{\rm pump} = -\left(\frac{n_{\rm eff}}{n}\right)_p \Gamma_p, \tag{12}$$

whose solution is simply

$$\Delta^{(1)}_{\rm pump}(t_p) = \Delta^{(1)}_{\rm pump}(t=0)e^{-\Gamma_p t_p} + \left(\frac{n_{\rm eff}}{n}\right)_p (-1 + e^{-\Gamma_p t_p}), \tag{13}$$

with the initial condition $\Delta^{(1)}_{\rm pump}(t=0) = 0$. For the following Ramsey interaction phase, according to Eq. (10), we can write

$$\Delta^{(1)}_{\rm Ramsey}(\Omega_\mu) = -\Delta^{(1)}_{\rm pump}(t_p)e^{-\gamma_2 T}\cos(\Omega_\mu \widetilde{T}), \tag{14}$$

where $\widetilde{T} = T + 4t_1/\pi$.

Under the hypothesis (7), the detection does not alter the atomic status so that Eq. (14) basically represents the population inversion at the beginning of the new pumping phase,

$$\Delta^{(2)}_{\rm pump}(t=0) \approx -\Delta^{(1)}_{\rm pump}(t_p)e^{-\gamma_2 T}\cos(\Omega_\mu \widetilde{T}). \tag{15}$$

At the beginning of a new pumping phase, the population inversion $\Delta^{(2)}_{\rm pump}(t=0)$ is then a function of the microwave detuning Ω_μ. In the ideal situation, this term is strongly reduced by the exponential factor $e^{-\Gamma_p t_p}$ [see Eq. (13)] so that, at the end of the pumping phase, the population inversion is a constant on the order of $-(\frac{n_{\rm eff}}{n})_p$. However, laser intensity and/or its duration may not guarantee this condition. In this case, it is easy to see that, for the RCF, we will have

$$\Delta^{(2)}_{\rm Ramsey}(\Omega_\mu) = -\Delta^{(1)}_{\rm pump}(t_p)e^{-\gamma_2 T}\cos(\Omega_\mu \widetilde{T}) \times [1 - e^{-\gamma_2 T - \Gamma_p t_p}\cos(\Omega_\mu \widetilde{T})], \tag{16}$$

and a second-harmonic component will appear on the signal. Specifically, the signal turns out [see Eq. (8) for a thin medium]

$$\Gamma'_p(L) = \Gamma'_p(0)\{1 - \zeta[1 + \overline{\Delta}_{\rm Ramsey}(\Omega_\mu)]\}, \tag{17}$$

where $\overline{\Delta}_{\rm Ramsey}(\Omega_\mu) = [\Delta^{(1)}_{\rm Ramsey}(\Omega_\mu) + \Delta^{(2)}_{\rm Ramsey}(\Omega_\mu)]/2$ is the average value of the contributions coming from the two cycles.

In Fig. 5, we report the behavior of $\Gamma'_p(L)$ given by Eq. (17) for a temperature of 318 K ($\zeta \approx 0.8$) and for different pumping times.

As observed in the experiments, the calculation confirms that reducing the pumping time implies a decreasing in the signal contrast as well, and at the same time, the RCF minimum appears increasingly flattened. We also notice that the emergence of high-order frequency components in the resonance curve is associated with a broadening of the resonance itself; in fact, the linewidth of the RCF of Fig. 4 is 157 Hz, slightly larger than the predicted value given by Eq. (11).

More in general, for very low laser power and/or pumping times, the memory effect may involve several cycles (let us say r), the Ramsey signal will be an average of the type,

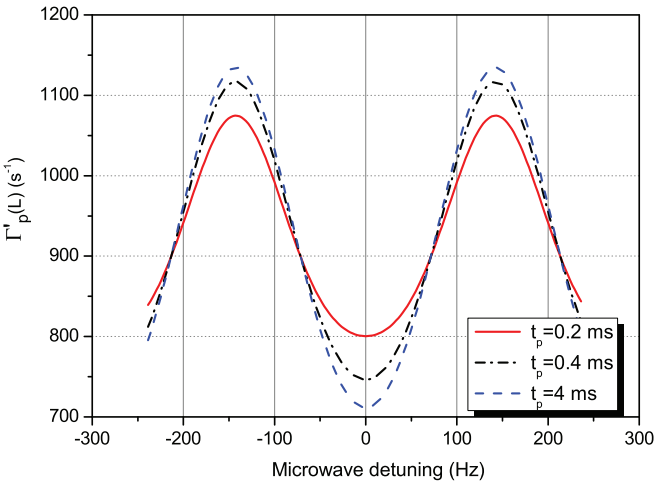

FIG. 5. (Color online) RCF calculated in the low-temperature regime; $T = 3$, $t_1 = 0.4$ ms, $\Gamma_p(0) = 20\,000$, and $\Gamma'_p(0) = 2000\ {\rm s}^{-1}$; dashed line: $t_p = 4$ ms; dashed-dotted line: $t_p = 0.4$ ms; continuous line: $t_p = 0.2$ ms.

$$\overline{\Delta}_{\rm Ramsey}(\Omega_\mu) = \frac{1}{r}\sum_{k=1}^{r} \Delta^{(k)}_{\rm Ramsey}(\Omega_\mu), \tag{18}$$

and higher-order harmonics will be present on the RCF.

Fitting the experimental points of Fig. 4 with a function of the type,

$$f(\Omega_\mu) = a_0 + a_1\cos(\Omega_\mu \widetilde{T}) + a_2\cos(2\,\Omega_\mu \widetilde{T}), \tag{19}$$

we find that the ratio a_2/a_1 turns out to be as large as 8.5%.

We notice that Fig. 3 refers to a pumping time $t_p = 4$ ms; in this case, the laser pulse area $\Gamma_p t_p$ is able to suppress the memory between one cycle and the successive one, and no higher-order harmonics are observed. In fact, fitting the experimental curve with Eq. (19), the amplitude of the second-harmonic component results less than 2%. This is not the case when t_p is much shorter as just described.

To avoid the memory effect, it is then required that the laser pulse area during the pumping phase satisfies the condition $\Gamma_p t_p \gg 1$. Although this condition can easily be satisfied for an optically thin medium, this could not be the case for a high-density atomic sample. In fact, due to absorption, not all the points of the cell are equally pumped, and the RCF may be influenced by a cycle memory effect for $t_p \approx \gamma_1^{-1}$ or larger.

An alternative approach consists of inserting a pause on the order of several γ_1^{-1} between the cycles. In this case, the relaxation induced by the buffer gas rebalances the atomic populations, and each cycle does not keep any memory of the previous interaction. In the same situation as Fig. 4, inserting a dead time of 20 ms between consecutive cycles, we experimentally observe that the Ramsey-fringe shape essentially reduces to that of Fig. 3.

It is expected that the cycle memory may affect the RCF as well in a high-temperature regime where, however, its effects may be masked by the nonlinearities related to the thickness of the atomic medium as described in the following section.

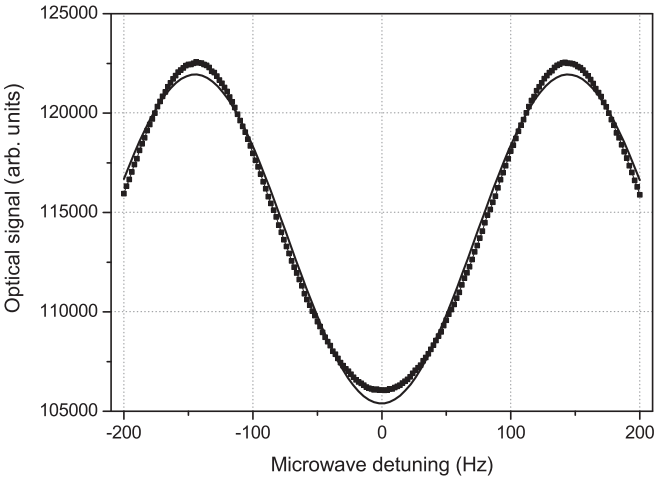

FIG. 6. RCF in the high-density regime (338 K); $t_p = 4$, $T = 3$, $t_1 = 0.4$, and $t_d = 0.15$ ms; dead time between consecutive cycles: 20 ms. The gray line is a fit of the data with a cosine function.

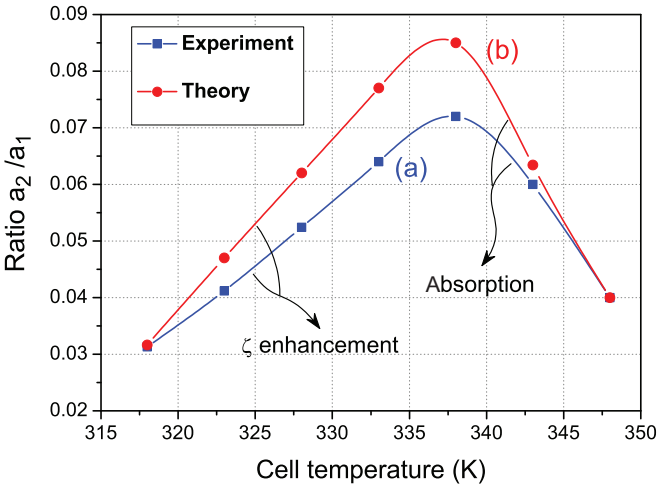

FIG. 7. (Color online) Ratio between the coefficients of second and first harmonics versus the cell temperature, (a) experiment and (b) theory.

C. High density

In this subsection, we will investigate the effects related to a thick atomic sample. Figure 6 refers to a RCF as detected at a temperature of 338 K. To assure that the operation cycles are well separated and to exclude that any modification of the line shape may be attributed to the memory effect, a dead time of 20 ms between consecutive cycles is included.

It is observed that, also in this case, the curve is not a pure cosine function, but the minimum appears flattened with respect the two side maxima, highlighting the presence of a second-harmonic component in the Ramsey signal. As in Fig. 4, the fit of the data with a cosine function does not reproduce the observed shape of the resonance line. To make this effect more evident, the experimental points have been interpolated with a curve of the type (19) and the ratio a_2/a_1 results of 7%.

We observed the RCF for different atomic densities, and through a nonlinear fit of the experimental curves, we inferred the amplitude of the second-harmonic component present on the signal. The result is shown in curve (a) of Fig. 7.

To theoretically explain this behavior, we perform a first preliminary step. In order to simplify the equations gaining at the same time in physical insight, we consider an intense laser pulse able to completely invert the ground-state population between the two clock levels in the entire cell so that

$$\Delta_{\text{pump}}(z) \approx -\left(\frac{n_{\text{eff}}}{n}\right)_p \quad \text{for each } z. \tag{20}$$

Supposing that condition (7) also holds for a thick medium, it is easy to see that the detection pumping rate Γ'_p can be written as

$$\Gamma'_p(L) = \Gamma'_p(0) e^{-\zeta[1+\Delta_{\text{Ramsey}}(\Omega_\mu)]}. \tag{21}$$

Taking Eqs. (10) and (20) into account, the previous relation becomes

$$\Gamma'_p(L) = \Gamma'_p(0) \exp\left\{-\zeta\left[1 + \left(\frac{n_{\text{eff}}}{n}\right)_p e^{-\gamma_2 T} \cos(\Omega_\mu \widetilde{T})\right]\right\}, \tag{22}$$

where we considered the RCF only of the total Ramsey pattern.

The emergence of high-order harmonics in the RCF is evident recalling that the exponential of a circular function can be expanded in terms of the modified Bessel function of the first type $I_k(x)$ with a k integer $\geqslant 0$ [20],

$$\Gamma'_p(L) = \Gamma'_p(0) e^{-\zeta}\left\{I_0(\chi) + 2\sum_{k=1}^{\infty} I_k(-\chi)\cos(k\Omega_\mu \widetilde{T})\right\}, \tag{23}$$

where $\chi = \zeta\left(\frac{n_{\text{eff}}}{n}\right)_p e^{-\gamma_2 T}$.

Since the $I_k(x)$'s are monotone functions of the argument, the amplitude of the high-order harmonics increases with the product $\zeta\left(\frac{n_e}{n}\right)_i$; then, this effect is proportional to the optical length of the cell and to the population inversion generated by the pumping light. We note, however, that γ_2 also increases with the atomic density due to the spin-exchange contribution [14], leading to a suppression of the effect above a certain density value and explaining the two different regimes observed in Fig. 7(a).

In the general case where the condition expressed by Eq. (20) is not satisfied, the set of Eqs. (4) can be solved numerically.

The ratio a_2/a_1 versus the cell temperature obtained by the numerical solution is reported in curve (b) of Fig. 7.

Up to about 333 K, the second-harmonic component amplitude increases due to the enhancement of the medium optical thickness ζ with temperature. Above that value, absorption and spin exchange prevail and overcome the pure density effect.

As for the memory effect previously described, we also notice that, in this case, the emergence of high-order harmonics in the line shape is associated with a linewidth broadening.

The higher-order components in the RCF, related to the atomic density, may appear relatively small. However, we point out that this nonlinear effect is greatly enhanced when a pumping technique, able to collect most of the atoms in only one of the two clock levels, is used (see, for example, Ref. [21]).

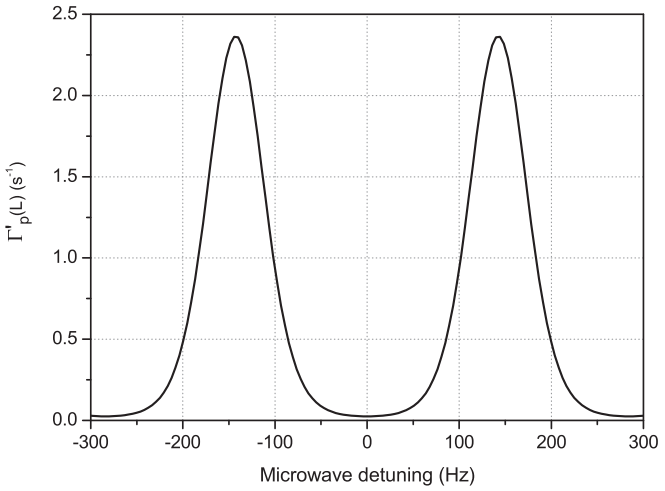

FIG. 8. Calculated RCF in the high-density regime and assuming a large population inversion at the end of the pumping phase; $a_2/a_1 \approx 0.5$, $a_3/a_1 \approx 0.16$, $a_4/a_1 \approx 0.4$.

Figure 8 shows the computed RCF at a temperature of 343 K ($\zeta \approx 9$) for the same values of laser intensities adopted in previous figures but assuming $(\frac{n_{\rm eff}}{n})_p = 0.9$. In this case, the ratio a_2/a_1 is about 50%, and third- and fourth-order harmonics (whose amplitudes are a_3 and a_4, respectively) are also required to reproduce the full curve well.

V. DISCUSSION AND CONCLUSIONS

In this paper, we described a few phenomena that may affect the line shape of the RCF observed in an atomic vapor cell with buffer gas.

The theoretical model, based on a simple three-level system with an appropriate rescaling of the parameters (pumping rate and atomic density), proved to be adequate to reproduce the observed experimental behavior of the resonances.

We observe that the two effects leading to the emergence of high-order harmonics in the RCF are, indeed, very different from a physical point of view. The cycle memory directly affects the atomic variables. To better clarify this concept, we recall that the observation of the clock transition can also be made by detecting the ground-state coherence under the form of a maser emission [18]. It is then easy to guess that an equation similar to Eq. (16) will hold for the coherence as well, leading to high-order harmonics in the RCF observed in the microwave domain. In other words, the cycle memory affects the line shape of the resonance through either population or coherence.

The high-density effects are, instead, related to the technique adopted to observe the resonance. The optical transmission signal is, in fact, represented by an "exponential filter" expressed by Eq. (22), which is responsible for the higher-order harmonics in the RCF as made clear by Eq. (23). On the contrary, provided the cycles are well separated, the atomic coherence is not affected by higher-order harmonics, and the detection of the maser signal is expected to be simply proportional to $\cos^2(\Omega_\mu \widetilde{T})$ [15].

We observe that the effects related to the emergence of high-order harmonics in the RCF are negligible in an atomic fountain. In fact, at each cycle, the atoms are renewed so that the interaction is intrinsically free of memory effect. Moreover, the atomic sample is diluted ($\zeta \ll 1$), and no phenomena related to the atomic density affect the line shape.

We finally point out that the phenomena we described in the paper modify the line shape symmetrically, therefore, they do not produce any frequency shift. However, their analysis is important since the shape of the resonance lines provides key information about the physical interactions experienced by the atoms.

[1] N. F. Ramsey, Phys. Rev **78**, 695 (1950).
[2] N. F. Ramsey, *Molecular Beams* (Oxford University Press, New York, 1956); J. E. Thomas, P. R. Hemmer, S. Ezekiel, C. C. Leiby, Jr., R. H. Picard, and C. R. Willis, Phys. Rev. Lett. **48**, 867 (1982); C. J. Bordé, C. Salomon, S. Avrillier, A. van Lerberghe, and C. Bréant, Phys. Rev. A **30**, 1836 (1984).
[3] M. A. Kasevich, E. Riis, S. Chu, and R. G. DeVoe, Phys. Rev. Lett. **63**, 612 (1989); F.-X. Esnault, D. Holleville, N. Rossetto, S. Guerandel, and N. Dimarcq, Phys. Rev. A **82**, 033436 (2010).
[4] V. Letchumanan, P. Gill, E. Riis, and A. G. Sinclair, Phys. Rev. A **70**, 033419 (2004); R. J. Rafac, B. C. Young, J. A. Beall, W. M. Itano, D. J. Wineland, and J. C. Bergquist, Phys. Rev. Lett **85**, 2462 (2000); L. Marmet and A. A. Madej, Can. J. Phys. **78**, 495 (2000).
[5] M. M. Salour and C. Cohen-Tannoudji, Phys. Rev. Lett. **38**, 757 (1977).
[6] B. Schuh, S. I. Kanorsky, A. Weis, and T. Hansch, Opt. Commun. **100**, 451 (1993).
[7] A. S. Zibrov, I. Novikova, and A. B. Matsko, Opt. Lett. **26**, 1311 (2001); A. S. Zibrov and A. B. Matsko, Phys. Rev. A **65**, 013814 (2001).
[8] M. Arditi and T. R. Carver, IEEE Trans. Instrum. Meas. **13**, 146 (1964).
[9] M. Merimaa, T. Lindvall, I. Tittonen, and E. Ikonen, J. Opt. Soc. Am B **20**, 273 (2003); T. Zanon, S. Guerandel, E. de Clercq, D. Holleville, N. Dimarcq, and A. Clairon, Phys. Rev. Lett. **94**, 193002 (2005); G. S. Pati, F. K. Fatemi, and M. S. Shahriar, Opt. Express **19**, 22388 (2011); P. Yun, Y. Zhang, G. Liu, W. Deng, L. You, and S. Gu, Europhys. Lett. **97**, 63004 (2012).
[10] B. Yan, Y. Ma, and Y. Wang, Phys. Rev. A **79**, 063820 (2009).
[11] S. Micalizio, A. Godone, F. Levi, and C. Calosso, Phys. Rev. A **79**, 013403 (2009).
[12] J. Lin, J. Deng, Y. Ma, H. He, and Y. Wang, Opt. Lett. **37**, 5036 (2012).
[13] S. Micalizio, C. E. Calosso, A. Godone, and F. Levi, Metrologia **49**, 425 (2012).
[14] J. Vanier and C. Audoin, *The Quantum Physics of Atomic Frequency Standards* (Hilger, Bristol, 1989).
[15] A. Godone, S. Micalizio, and F. Levi, Phys. Rev. A **70**, 023409 (2004).

[16] E. I. Alekseyev, Y. N. Bazarov, and G. I. Telegin, Radio Eng. Electron. Phys. **20**, 73 (1975); E. I. Alekseyev, Y. N. Bazarov, and A. E. Levishin, *ibid*. **19**, 77 (1974).

[17] X. Liu, J.-M. Merolla, S. Guerandel, C. Gorecki, E. de Clercq, and R. Boudot, Phys. Rev. A **87**, 013416 (2013).

[18] A. Godone, S. Micalizio, F. Levi, and C. Calosso, Phys. Rev. A **74**, 043401 (2006).

[19] G. Kramer, in *Proceedings of the Conference on Precision Electromagnetic Measurements, London, 1974* (IEE, Luxembourg, 1974), p. 157; A. Joyet, G. Mileti, G. Dudle, and P. Thomann, IEEE Trans. Instrum. Meas. **50**, 150 (2001).

[20] *Handbook of Mathematical Functions With Formulas, Graphs, and Mathematical Tables*, edited by M. Abramowitz and I. A. Stegun (Dover, Mineola, NY, 1972), Vol. 55, tenth printing.

[21] N. D. Bhaskar, Phys. Rev. A **47**, R4559 (1993); S. Micalizio, A. Godone, F. Levi, and C. Calosso, *ibid.* **80**, 023419 (2009).